Article

Cell Reports

Cell Competition Promotes Phenotypically Silent Cardiomyocyte Replacement in the Mammalian Heart

Graphical Abstract

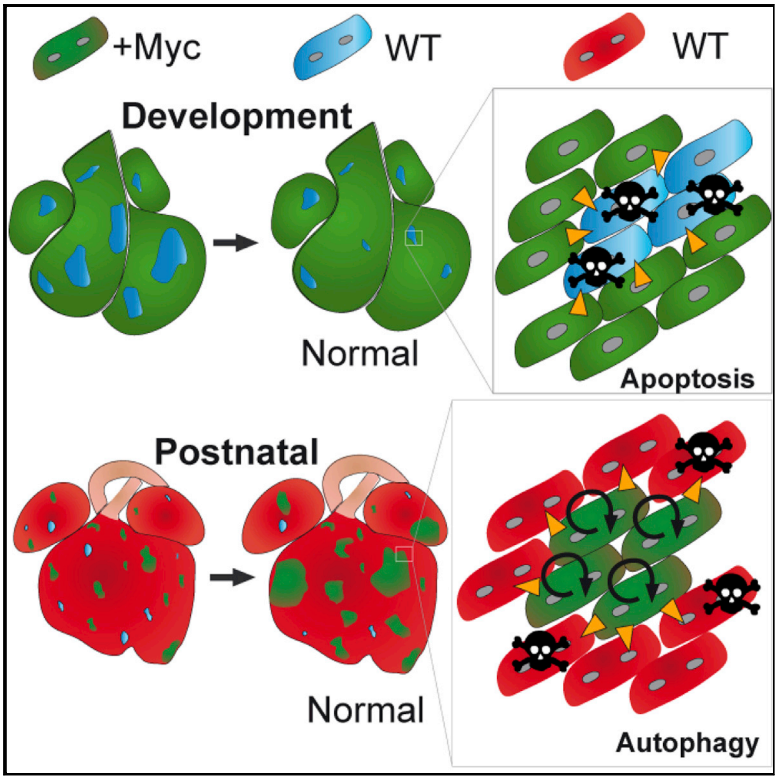

Highlights

Cardiomyocytes are sensitive to Myc-induced competition in development and adult life

Cardiomyocyte competition is driven by short-range interactions leading to cell death

Cardiomyocyte replacement by cell competition is phenotypically silent

Authors

Cristina Villa del Campo, Cristina Clavería, Rocío Sierra, Miguel Torres

Correspondence

mtorres@cnic.es

In Brief

Cardiomyocytes of the mammalian heart are generated during prenatal and early postnatal development and show very low turnover during adult life. Strategies for cardiomyocyte generation and replacement are therefore essential for repairing the diseased heart. Villa del Campo et al. show that mosaic Myc overexpression in cardiomyocytes leads to the phenotypically silent replacement of normal cardiomyocytes by the Myc-overexpressing ones, through a process known as cell competition. This work uncovers a mechanism potentially relevant to cardiac repair.

Accession Numbers

GSE58858

Villa del Campo et al., 2014, Cell Reports 8, 1741–1751
September 25, 2014 ©2014 The Authors
http://dx.doi.org/10.1016/j.celrep.2014.08.005

Cell Reports
Article

Cell Competition Promotes Phenotypically Silent Cardiomyocyte Replacement in the Mammalian Heart

Cristina Villa del Campo,[1] Cristina Clavería,[1] Rocío Sierra,[1] and Miguel Torres[1,*]
[1]Departamento de Desarrollo y Reparación Cardiovascular, Centro Nacional de Investigaciones Cardiovasculares (CNIC), c/ Melchor Fernández Almagro, 3, E-28029 Madrid, Spain
*Correspondence: mtorres@cnic.es
http://dx.doi.org/10.1016/j.celrep.2014.08.005

SUMMARY

Heterogeneous anabolic capacity in cell populations can trigger a phenomenon known as cell competition, through which less active cells are eliminated. Cell competition has been induced experimentally in stem/precursor cell populations in insects and mammals and takes place endogenously in early mouse embryonic cells. Here, we show that cell competition can be efficiently induced in mouse cardiomyocytes by mosaic overexpression of *Myc* during both gestation and adult life. The expansion of the *Myc*-overexpressing cardiomyocyte population is driven by the elimination of wild-type cardiomyocytes. Importantly, this cardiomyocyte replacement is phenotypically silent and does not affect heart anatomy or function. These results show that the capacity for cell competition in mammals is not restricted to stem cell populations and suggest that stimulated cell competition has potential as a cardiomyocyte-replacement strategy.

INTRODUCTION

Cell competition is a mechanism that eliminates suboptimal cells from tissues when "fitter" cells are present (reviewed in Baker, 2011; de Beco et al., 2012; Levayer and Moreno, 2013; Vincent et al., 2013). Cell-to-cell heterogeneity in anabolic capacity led to the first description of cell competition, during *Drosophila* development (Morata and Ripoll, 1975), and is currently the most frequent feature found associated with this phenomenon. The fluctuations in anabolic capacity that trigger cell competition are within a physiological range, and "loser" cells are viable and capable, in the absence of fitter cells, of sustaining tissue growth and performance. Cell competition can thus be envisioned as an optimization mechanism enabling tissues to achieve their best possible cellular composition by favoring the fitter cell population at the expense of less-fit cells. Cell competition can be experimentally induced by generating loser cells through the mosaic reduction of cell anabolism (Morata and Ripoll, 1975) or by generating "winner" cells through the mosaic increase of cell anabolism (supercompetition) (de la Cova et al., 2004; Moreno and Basler, 2004). The conserved cell anabolism regulator Myc is involved in cell growth and proliferation (reviewed in Dang, 2013; Gallant, 2013; Levens, 2013) and plays essential roles in mammalian development (Davis et al., 1993; reviewed in Hurlin, 2013). Moderate increase in Myc levels in a mosaic fashion in *Drosophila* imaginal discs (de la Cova et al., 2004; Moreno and Basler, 2004) and pregastrulation mammalian embryos (Clavería et al., 2013) induces supercompetition, leading to the phenotypically silent replacement of wild-type cells by Myc-overexpressing cells without overt phenotypic consequences. In addition, natural Myc fluctuations trigger cell competition in the mouse epiblast (Clavería et al., 2013), indicating an endogenous role for cell competition in optimization of the pool of precursor cells that generate the embryo. Mosaic Myc overexpression also induces cell supercompetition in embryonic stem cell cultures (Clavería et al., 2013; Sancho et al., 2013), and hematopoietic stem cells have been shown to undergo p53-dependent cell competition (Bondar and Medzhitov, 2010; Marusyk et al., 2010). These observations suggest that the capacity for cell competition might be associated with stemness, but this hypothesis has not been tested. Here, we explored this issue by asking whether cell competition could be induced in one of the first lineages to differentiate in the mammalian embryo, the cardiac lineage.

Cardiac precursors originate early in gastrulation within the anteriormost embryonic mesoderm (reviewed in Vincent and Buckingham, 2010). During mouse gastrulation, cardiac precursors migrate anteriorly and form a cardiac crescent, which by embryonic day 8.0 (E8.0) has folded into a primary tube containing still-proliferative but differentiated and functionally active cardiomyocytes (reviewed in Evans et al., 2010; Rana et al., 2013). A subset of cardiac precursors remain undifferentiated in the second heart field (Kelly et al., 2001) and are progressively added to the heart tube until cardiac chambers and outflow and inflow tracts are definitively laid down around E10. After birth, most cardiomyocytes stop dividing and undergo hypertrophy to establish the mature definitive myocardium (Soonpaa et al., 1996). Here, we show that mosaic Myc overexpression in cardiomyocytes at levels that do not alter heart anatomy or function promote the phenotypically silent replacement of wild-type (WT) cardiomyocytes in the mouse fetal and adult myocardium through cell competition. Our results show the widespread ability of mammalian cells to undergo Myc-driven cell competition and identify cell competition as an efficient mechanism for phenotypically silent substitution of cell populations while preserving organ function.

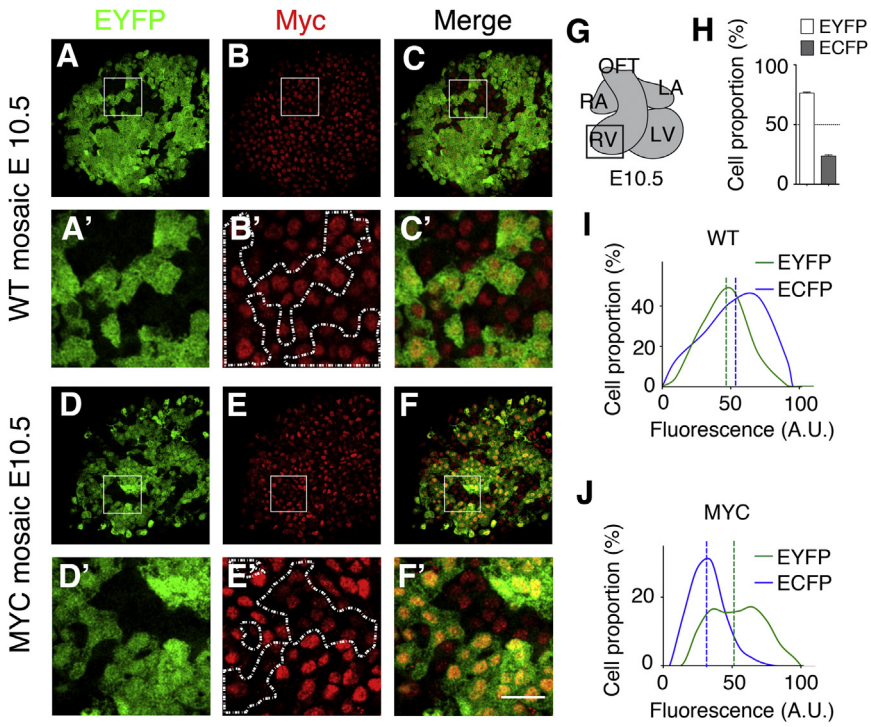

Figure 1. Mosaic Myc Overexpression Driven by Nkx2.5Cre in the Developing Heart

(A–C) Confocal sections showing EYFP$^+$ cardiomyocyte distribution and Myc expression by immunofluorescence in the right ventricle of a whole-mount *Nkx2.5Cre*-recombined *iMOS*^{WT} E10.5 heart (WT), as depicted in (G). (A′)–(C′) show magnified details of the boxed areas in (A)–(C).

(D–F′) Similar data for the *Nkx2.5Cre*-recombined *iMOS*$^{T1\text{-}Myc}$ E10.5 heart (MYC). Scale bar, 50 μm. Dashed lines in (B′) and (E′) outline the frontiers between EYFP$^+$ and EYFP$^-$ cells. ECFP fluorescence is lost upon Myc immunodetection; however, all EYFP$^-$ cells are ECFP$^+$ (see Figure 2).

(G) Schematic representation of an E10.5 heart identifying the area shown in A-F′. OFT, outflow tract; RA, right atrium; LA, left atrium; RV, right ventricle; LV, left ventricle.

(H) Graph showing the proportions observed of EYFP and ECFP cardiomyocytes in *Nkx2.5Cre*-recombined *iMOS*^{WT} E10.5 whole hearts (n = 7). Data are means ± SEM.

(I and J) Distribution of Myc protein levels in the EYFP and ECFP cell populations of *iMOS*^{WT} (I) and *iMOS*$^{T1\text{-}Myc}$ (J) mosaic whole hearts at E10.5; Myc protein levels were quantified from the immunofluorescence images similar to those in (A)–(F′). n = 425 cells in (I) and 449 in (J). Dashed vertical lines indicate the mean for each distribution.

RESULTS

Mosaic *Myc* Overexpression Induces Cardiomyocyte Population Expansion in the Developing Heart

To test the consequences of overexpressing *Myc* in the developing heart, we used the recently established *iMOS* system (Clavería et al., 2013), which allows the Cre-mediated conditional induction of random genetic mosaics. We first generated control random genetic mosaics in cardiac lineages using *Nkx2.5-Cre* (Stanley et al., 2002) to induce the *iMOS*^{WT} transgene, which produces a random mosaic of enhanced yellow fluorescent protein (EYFP) and enhanced cyan fluorescent protein (ECFP) WT cells. Quantitative confocal analysis of *iMOS*^{WT} recombination at E10.5 in *iMOS*^{WT}; *Nkx2.5-Cre* hearts confirmed the mosaic expression pattern of the two reporter proteins in embryonic cardiomyocytes at a reproducible cell population ratio, as previously described (EYFP:ECFP = 3:1) (Figures 1A–1C, 1G, and 1H). Again as described (Stanley et al., 2002), the fluorescent protein distribution pattern indicated *iMOS* activation throughout the embryonic heart (Figures 1A–1C′). We then generated *Nkx2.5-Cre*-induced *iMOS*$^{T1\text{-}Myc}$ mosaics, in which the EYFP cell population moderately overexpresses *Myc* (Clavería et al., 2013) (Figures 1D–1F′). Confocal analysis of EYFP simultaneously with MYC protein immunodetection showed the expected increase in MYC levels in the EYFP cell population of *iMOS*$^{T1\text{-}Myc}$ mosaics, but not *iMOS*^{WT} mosaics (Figures 1I and 1J). We then quantified the contribution of the mosaic cell populations by confocal analysis at different stages of heart development. In the *iMOS*$^{T1\text{-}Myc}$ mosaics we found a progressive reduction in the relative abundance of the ECFP-WT cell population —and a concomitantly increased relative abundance of the EYFP-Myc population— that was not observed in the *iMOS*^{WT} mosaics (Figures 2A–2G). The proportion of ECFP cardiomyocytes at E9.5 in *iMOS*$^{T1\text{-}Myc}$ mosaics was lower (but not significantly) than that observed in *iMOS*^{WT} mosaics. From then on, the relative abundance of the ECFP-WT population in *iMOS*$^{T1\text{-}Myc}$ mosaics showed a progressive decline to 60% of the *iMOS*^{WT} value at E10.5, 40% at E11.5, and 25% at postnatal day 0 (P0) (Figure 2G). The shift in cell populations thus takes place mostly in a narrow time window between E9.5 and E11.5.

Previous studies showed that Myc overexpression in cardiomyocytes during fetal life can lead to pathological cardiac hyperplasia (Jackson et al., 1990). However, in these studies, Myc expression was 20-fold above normal. To determine whether the overexpression levels used here could lead to cardiac hyperplasia we characterized adult heart anatomy and cardiomyocyte size. P0 hearts from *Nkx2.5-Cre*-recombined *iMOS*$^{T1\text{-}Myc}$ and *iMOS*^{WT} mice were of normal size and anatomy (Figures S1A and S1B and data not shown), and cardiomyocytes from the *iMOS*$^{T1\text{-}Myc}$ hearts were of a similar size to those from *iMOS*^{WT} hearts (Figure S1C).

The shift in the cell population proportion observed in *iMOS*^{WT} mosaics thus results from expansion of the EYFP *Myc*-overexpressing cardiomyocyte population and a concomitant reduction of the ECFP WT population relative contribution, without disruption of heart cell composition or anatomy. These results also indicate that the levels of *Myc* overexpression from the *iMOS*$^{T1\text{-}Myc}$ allele are within the limits that allow normal cardiomyocyte development and do not provoke hyperplasia.

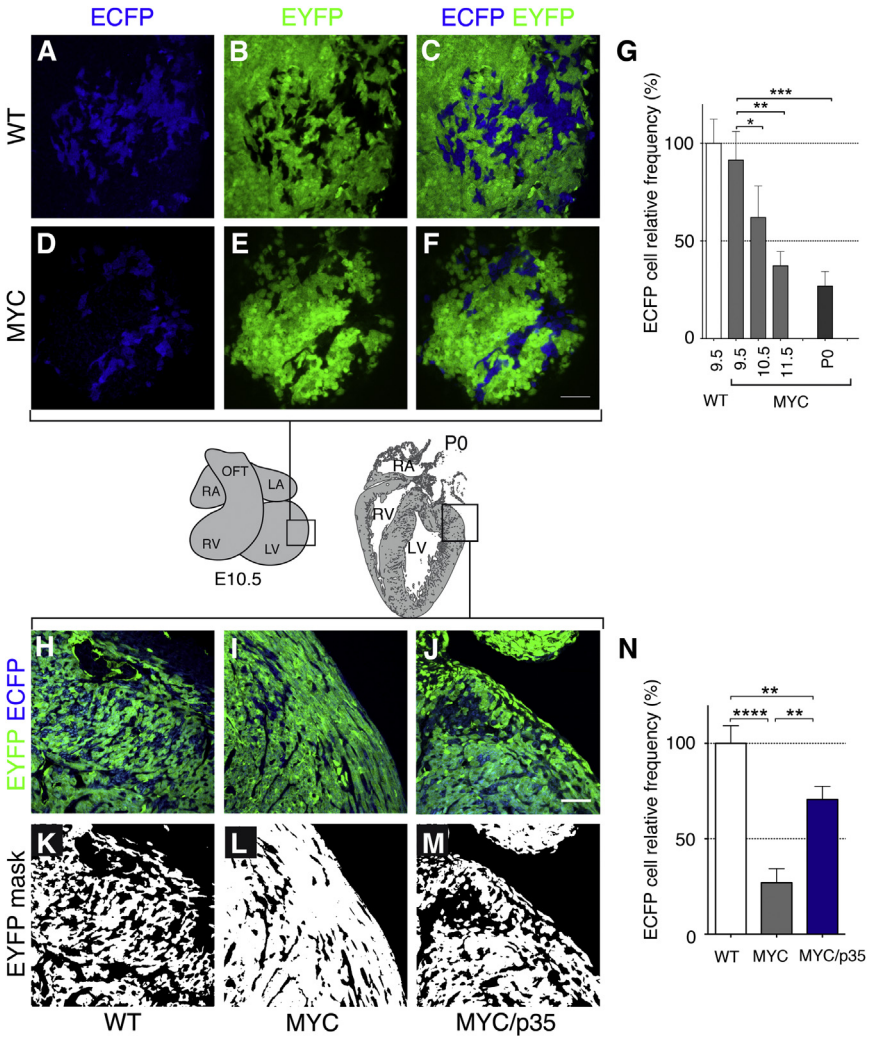

Figure 2. The Myc-Overexpressing Cardiomyocyte Population Expands in the Developing Heart

(A–F) Confocal sections showing EYFP$^+$ and ECFP$^+$ cardiomyocyte distributions in the left ventricle of whole-mount E10.5 hearts from *Nkx2.5Cre*-recombined *iMOS*^{WT} (WT) (A–C) and *iMOS*$^{T1\text{-}Myc}$ (MYC) (D–F) embryos. Scale bar, 50 μm.

(G) Percentage ECFP$^+$ area at different embryonic stages in whole hearts of the *iMOS*$^{T1\text{-}Myc}$ (MYC) mosaics relative to that observed in the *iMOS*^{WT} (WT) mosaics, which was normalized to 100%. Numbers on the x axis indicate the day of embryonic development; P0 indicates postnatal day 0 ($n \geq 5$ embryos).

(H–J) Confocal detection of EYFP$^+$ and ECFP$^+$ cardiomyocyte distributions in histological sections of the left ventricle of P0 hearts from *Nkx2.5Cre*-recombined *iMOS*^{WT} (WT) (H), *iMOS*$^{T1\text{-}Myc}$ (MYC) (I), and *iMOS*$^{T1\text{-}Myc/T2\text{-}p35}$ (MYC/p35) mice. Scale bar, 50 μm.

(K–M) show masks of the EYFP detection in (H) and (I).

(N) Percentage of ECFP$^+$ cells observed at P0 in whole hearts of the *iMOS*$^{T1\text{-}Myc}$ (MYC) and *iMOS*^{WT} (WT) mosaics relative to that observed in the *iMOS*^{WT} (WT) mosaics, which was normalized to 100%.

For ease of comparison, data for ECFP proportion in MYC mosaics at P0 is repeated in (G) and (N). $n \geq 4$). Data in (G) and (N) are means ± SEM; *$p < 0.05$; **$p < 0.01$; ***$p < 0.001$.

Islet-1 Progenitors Are Highly Sensitive to *Myc*-Induced Cell Competition

We next explored the impact of inducing *Myc* mosaicism in Islet1$^+$ cardiac progenitors. For this, we generated *iMOS*$^{T1\text{-}Myc}$ mosaics in second heart field (SHF) progenitors using *Islet1-Cre* (Yang et al., 2006). This Cre driver provides partial interspersed recombination of the SHF cell population, resulting in about 7% EYFP recombined cardiomyocytes in the right ventricle (RV) of *iMOS*^{WT} mosaics (Figures 3A, 3D, 3E, and 3E′). In contrast, the RV of *iMOS* $^{T1\text{-}Myc}$*; Islet1-Cre* hearts on average contained 40% EYFP cardiomyocytes at P0, representing a 5.7-fold expansion during gestation of the original EYFP cardiomyocyte population (Figures 3B, 3D, 3F, and 3F′). In addition, the ECFP cardiomyocyte population in the *Islet-Cre*-induced *iMOS*$^{T1\text{-}Myc}$ mosaic hearts was almost completely eliminated by P0 (Figures 3E′, 3F′, and 3H). These results indicate a more active elimination of the mosaic ECFP-WT cell population and a continued expansion of the *Myc*-overexpressing cardiomyocyte population during fetal life, in a context in which it is continuously confronted with WT cardiomyocytes. We then characterized the temporal progression of ECFP cardiomyocyte depletion in *iMOS*$^{T1\text{-}Myc}$ mosaics, finding that this population was already reduced to 40% of its original contribution by E9.5, with further progressive reduction until the final residual presence at birth (Figures 3I–3L). The enhanced early elimination of WT progenitors in the *Islet-Cre*-induced mosaics indicates that undifferentiated Islet1$^+$ cardiac progenitors are highly sensitive to *Myc* mosaicism.

The *Myc*-Overexpressing Cardiomyocyte Population Expands by Apoptosis-Driven Cell Competition

To study the mechanisms underlying the expansion of the *Myc*-overexpressing cardiomyocyte population during development, we first determined the abundance of PHH3$^+$ cells and bromodeoxyuridine (BrdU) incorporation in *iMOS* mosaics at E10.5, when the shift in the cell population proportion is taking place. Overall, PHH3$^+$ and BrdU$^+$ cell frequencies did not differ significantly between *iMOS*$^{T1\text{-}Myc}$ and *iMOS*^{WT} cardiomyocytes (Figure S2). Moreover, the PHH3$^+$ and BrdU$^+$ cell frequencies in the EYFP cell population of *iMOS*$^{T1\text{-}Myc}$ mosaics was not different from that in the ECFP population (Figures S2D and S2E). These results fit with previous studies showing that the *Myc* dosage induced by a single *Rosa26* allele does not increase proliferation rates in most tissues (Clavería et al., 2013; Murphy

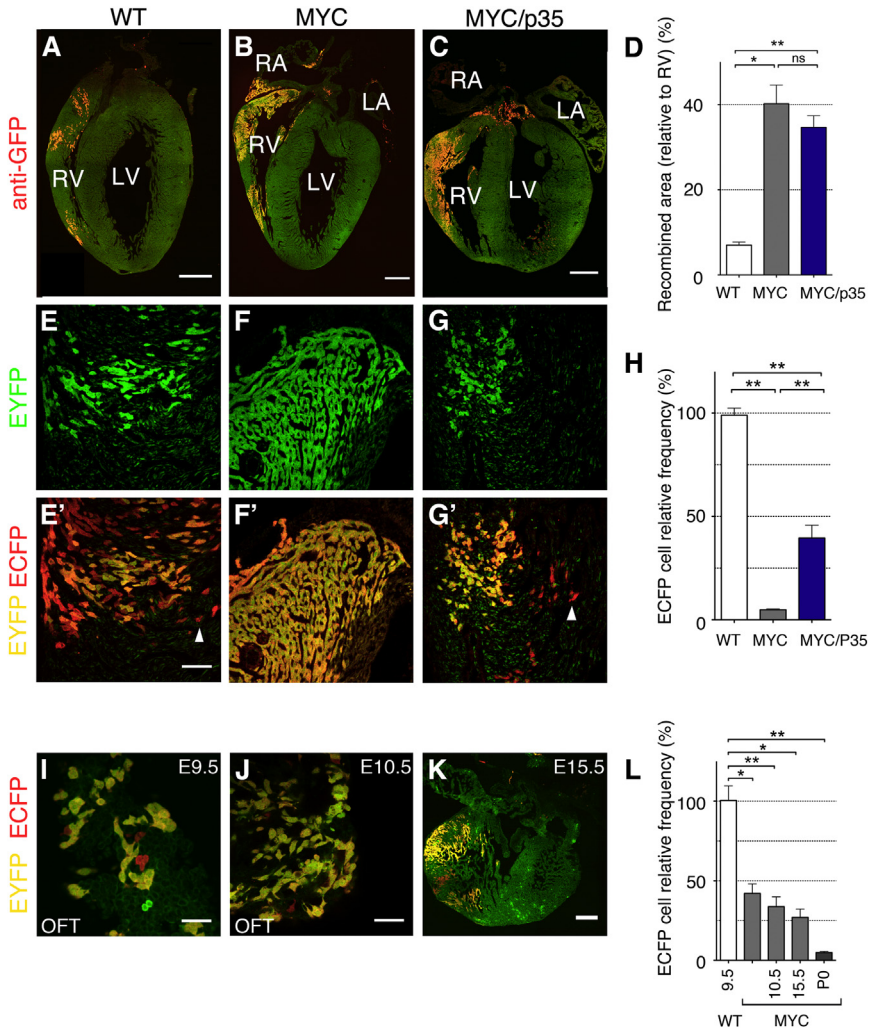

Figure 3. Enhanced Expansion of Myc-Overexpressing Cardiomyocytes upon Mosaic Induction in Islet-1^{+} Progenitors

(A–G′) Confocal detection of EYFP^{+} (A–C), anti-GFP immunofluorescence (detecting both EYFP and ECFP) (E–G) and colocalization of both signals (E′–G′) in histological sections from *Islet1Cre*-recombined *iMOS^{WT}* (WT) (A, E, and E′), *iMOS$^{T1\text{-}Myc}$* (MYC) (B, F, and F′), and *iMOS$^{T1\text{-}Myc/T2\text{-}p35}$* (MYC/p35) newborn mice. In (E′)–(G′), EYFP^{+} cells are yellow because they are positive for both EYFP and anti-GFP, and ECFP^{+} cells are detected in red, as they are only positive for anti-GFP. Scale bar, 100 μm for (A)–(C) and 50 μm for (E′). RA, right atrium; LA, left atrium; RV, right ventricle; LV, left ventricle. (D) Percentage of the RV area positive for anti-GFP immunofluorescence in *Islet1Cre*-recombined *iMOS^{WT}* (WT), *iMOS$^{T1\text{-}Myc}$* (MYC), and *iMOS$^{T1\text{-}Myc/T2\text{-}p35}$* (MYC/p35) newborn mice ($n \geq 4$).

(H) Percentage of ECFP^{+} recombined area with respect to the total EYFP+ECFP-recombined area observed at P0 in the *iMOS$^{T1\text{-}Myc}$* (MYC) and *iMOS$^{T1\text{-}Myc/T2\text{-}p35}$* (MYC/p35) mosaics relative to that observed in the *iMOS^{WT}* (WT) mosaics, which was normalized to 100% ($n \geq 4$).

(I–K) Confocal sections of the E9.5 (I) and E10.5 (J) OFT and the E15.5 RV (K) from *Islet1Cre*-recombined *iMOS$^{T1\text{-}Myc}$* hearts, showing overlays of EYFP and anti-GFP signals. Scale bar, 50 μm for I and J and 100 μm for (K).

(L) Percentage of ECFP^{+} area with respect to the total EYFP+ECFP-recombined area observed at different stages in the *iMOS$^{T1\text{-}Myc}$* (MYC) mosaics relative to that observed in the *iMOS^{WT}* (WT) mosaics, which was normalized to 100%. Numbers on the x axis indicate the day of embryonic development; P0 indicates postnatal day 0 ($n \geq 4$). For ease of comparison, data for ECFP proportion in MYC mosaics at P0 are repeated in (H) and (L). Data in (D), (H), and (L) are means ± SEM. *$p < 0.05$; **$p < 0.01$; ***$p > 0.001$.

et al., 2008) and suggest that the shift in cardiomyocyte populations is not produced by overt differences in cell proliferation between the two cell populations.

To evaluate the role of cell death in the depletion of WT cardiomyocytes, we generated mosaics of the *iMOS$^{T1\text{-}Myc/T2p35}$* strain, which produces a random mosaic of EYFP-*Myc* and ECFP-*p35* cells. p35 is a baculoviral caspase inhibitor able to prevent apoptosis in insects and mammals (Clavería et al., 1998; Hay et al., 1994). Quantitative confocal analysis of P0 hearts from *iMOS$^{T1\text{-}Myc/T2p35}$* mosaics induced with either *Nkx2.5-Cre* or *Islet1-Cre* showed that the p35-expressing ECFP population was substantially, although not completely, protected against elimination (Figures 2H–2N, 3C, and 3G–3H). This result indicates that cell death is a predominant mechanism in the population shift observed in *iMOS$^{T1\text{-}Myc}$* mosaics. However, expansion of the EYFP-Myc cell population did not differ significantly between *Islet1-Cre*-induced *iMOS$^{T1\text{-}Myc/T2p35}$* and *iMOS $^{T1\text{-}Myc}$* mosaics (Figure 3D), indicating that expansion of *Myc*-enriched cardiomyocytes can progress through elimination of nonrecombined WT cardiomyocytes even when small numbers of apoptosis-resistant ECFP-p35 cardiomyocytes are present.

We next scored apoptosis by TUNEL at E10.5 in the *Nkx2.5-Cre*-induced mosaics, concentrating on the outflow tract (OFT) because this region had higher rates of apoptosis in the *iMOS^{WT}* mosaics. The *iMOS$^{T1\text{-}Myc}$* mosaics had a 5-fold higher overall apoptosis rate than *iMOS^{WT}* mosaics (Figures 4A–4C). Furthermore, the apoptosis rate in ECFP-WT cells of the *iMOS$^{T1\text{-}Myc}$* mosaic was markedly higher than observed in the EYFP-*Myc* cells (Figures 4D–4F). Interestingly, the apoptosis rate varied between heart regions: whereas the ECFP/EYFP TUNEL ratio was 4- to 5-fold above baseline in the ventricles, in the OFT it was over 10-fold higher, indicating that ECFP-WT cardiomyocytes in this region are especially sensitive to mosaic *Myc* overexpression.

To study the range limit of the cellular interaction leading to ECFP-WT cardiomyocyte apoptosis in *iMOS$^{T1\text{-}Myc}$* mosaics, we took advantage of the *Islet-Cre* strain. The low-rate, interspersed recombination induced by this line allowed us to score apoptosis separately for WT cardiomyocytes in direct contact

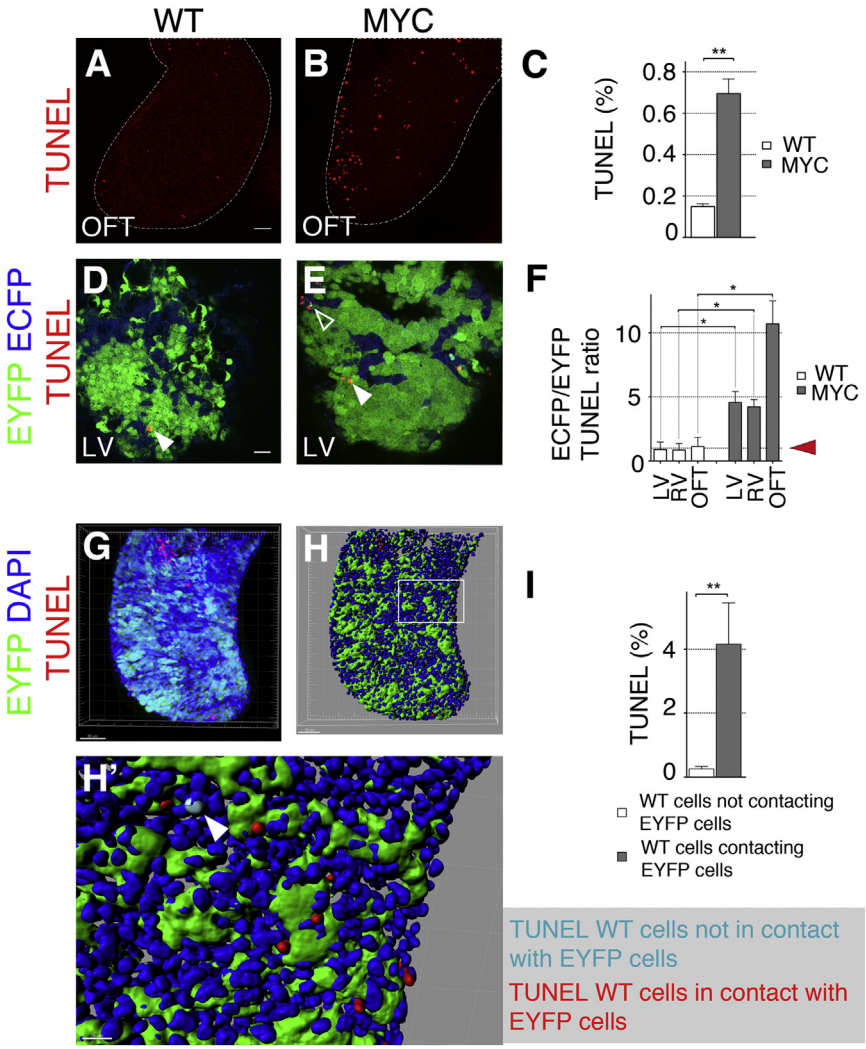

Figure 4. Myc-Overexpressing Cardiomyocytes Expand by Inducing Apoptosis of Neighboring WT Cardiomyocytes

(A and B) Maximal projections of confocal stacks (30 μm deep) from the OFT region of *Nkx2.5Cre*-recombined *iMOS*^{WT} (WT) (A) and *iMOS*$^{T1\text{-}Myc}$ (MYC) (B) whole-mount TUNEL-stained E10.5 hearts. Scale bar, 50 μm.

(C) TUNEL staining frequency in cardiomyocytes from the mosaics shown in (A) and (B) (n = 4 WT and 7 MYC mosaics).

(D and E) Confocal sections from the left ventricle (LV) of *Nkx2.5Cre*-recombined *iMOS*^{WT} (WT) (D) and *iMOS*$^{T1\text{-}Myc}$ (MYC) (E) whole-mount TUNEL-stained E10.5 hearts, showing overlaid EYFP, ECFP, and TUNEL signals. Filled arrowheads point to EYFP^{+} TUNEL^{+} cells and empty arrowheads to ECFP^{+} TUNEL^{+} cells. Scale bar, 50 μm.

(F) ECFP/EYFP TUNEL frequency ratios in different regions of *Nkx2.5Cre*-recombined *iMOS*^{WT} (WT) and *iMOS*$^{T1\text{-}Myc}$ (MYC) whole-mount E10.5 hearts (n = 4 WT and 7 MYC mosaics). LV, left ventricle; RV, right ventricle; OFT, outflow tract. Arrowhead marks the unbiased ECFP/EYFP TUNEL frequency ratio = 1.

(G) Maximal projection of the OFT from an *Islet1-MerCreMer*-recombined *iMOS*$^{T1\text{-}Myc}$ E10.5 heart (MYC), showing overlaid EYFP, DAPI and TUNEL signals. Scale bar, 70 μm.

(H) Computer 3D reconstruction of the stack shown in (G).

(H′) Magnification of the boxed region in (H), showing TUNEL+ WT cells contacting (red) and not contacting (light blue, arrowhead) MYC-overexpressing cells. Scale bar, 20 μm.

(I) TUNEL frequency in WT cells contacting and not contacting EYFP cells in *Islet1MerCreMer*-recombined *iMOS*$^{T1\text{-}Myc}$ E10.5 hearts (MYC) (N = 3 and ≥ 2,815 cells).

Data in (C), (F), and (I) are means ± SEM. *p < 0.05; **p < 0.01; ***p < 0.001.

with EYFP cells and those not in contact (Figures 4G–4H′). Apoptosis was 17-fold more frequent in WT cardiomyocytes in direct contact with *Myc*-overexpressing EYFP cardiomyocytes than in those not contacting EYFP cardiomyocytes (Figure 4I; Movie S1).

These results indicate that the expansion of *Myc*-overexpressing cardiomyocytes requires the elimination of neighboring WT cardiomyocytes through apoptosis triggered by direct cell-cell contact or short-range signaling. Our characterization thus establishes that the replacement of the WT cardiomyocyte population by the Myc-overexpressing population is due to apoptosis-driven cell competition.

Myc Overexpression Induces Cardiomyocyte Population Expansion in the Adult Heart

To determine whether increased *Myc* levels impact cardiomyocyte population homeostasis during adult life, we induced mosaicism in the adult cardiomyocyte population by using the tamoxifen-inducible *αMHC-merCremer* strain (Sohal et al., 2001) (Figure 5A). Mosaics were induced by feeding animals tamoxifen during the first month after weaning, and hearts were analyzed immediately after tamoxifen cessation and at subsequent intervals up to 1 year (Figure 5A). This protocol produced an initial EYFP recombination slightly above 50% (Figure 6D). Previous studies have shown that strong Myc overexpression in cardiomyocytes of adult mice induces cardiomyocyte hypertrophy (Xiao et al., 2001). We thus first analyzed whether hypertrophy also resulted from long-term moderate *Myc* overexpression. Tamoxifen-induced adult *iMOS*$^{T1\text{-}Myc}$ and *iMOS*^{WT} mice showed no spontaneous cardiac malfunction and their hearts were of normal size and anatomy even after 2 months of an intense exercise protocol (Figures 5B–5E). Measurement of average cardiomyocyte 2D size, both in histological sections and in cultures of disaggregated cardiac cells (Figures 5F–5I), showed that cardiomyocytes in *iMOS*$^{T1\text{-}Myc}$ hearts were not only not bigger than those in *iMOS*^{WT} hearts but also in fact slightly smaller (Figure 5J). Due to binucleation, adult cardiomyocytes could contain more that one *EYFP-Myc* copy, and the levels of EYFP are expected to correlate with the *Myc* dose in the *iMOS*$^{T1\text{-}Myc}$ mosaics. Analysis of per-cell cardiomyocyte size and EYFP level showed no

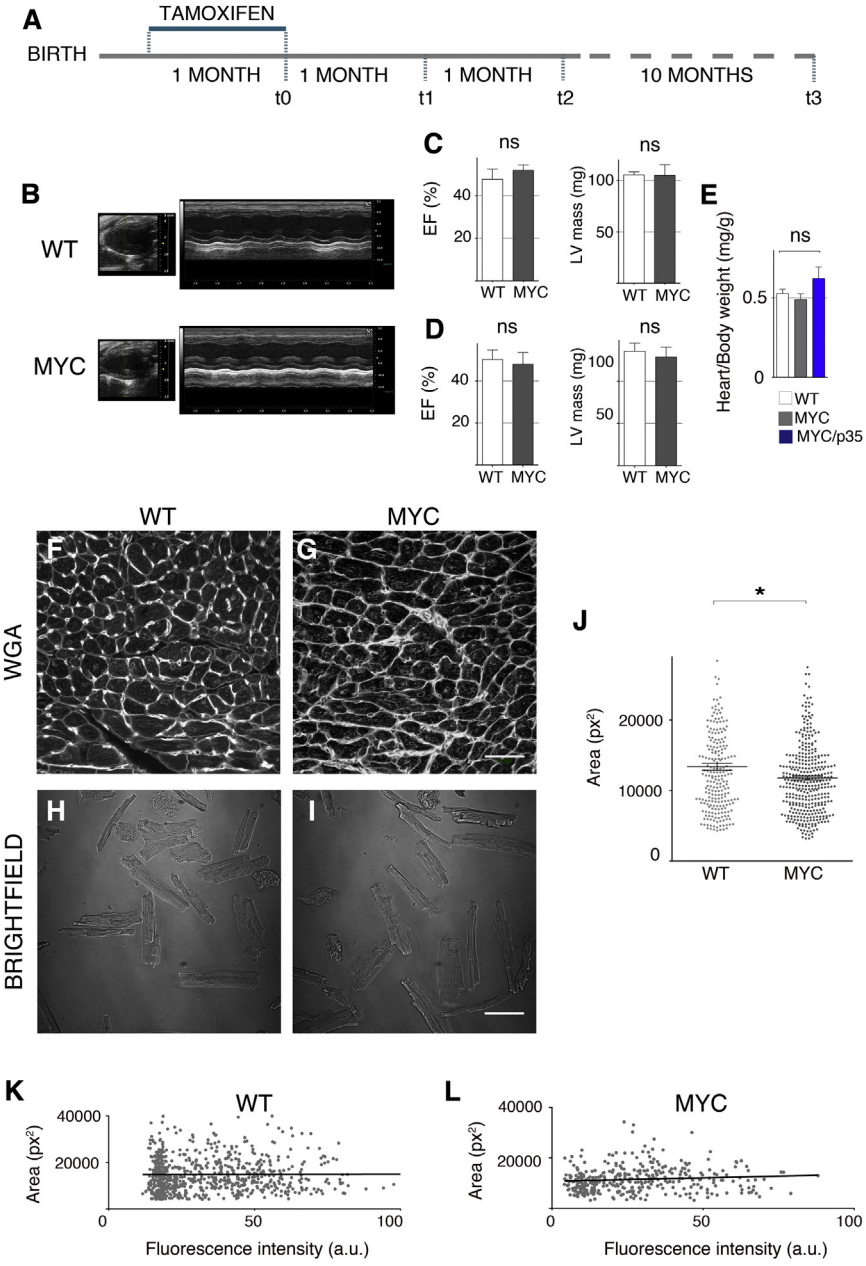

Figure 5. Mosaic MYC Overexpression in Adult Cardiomyocytes Is Phenotypically Silent

(A) αMHCmerCremer-recombined *iMOS*$^{T1\text{-}Myc}$ mosaics and control littermates were treated as schematized for experiments in (B)–(L) and in Figure 6.

(B) Long axis M-mode echocardiography image from an *iMOS*$^{T1\text{-}Myc}$ (MYC) mosaic WT littermate at t2.

(C) Graphs show ejection fraction (EF) and left ventricle (LV) mass from the echocardiographic study in the *iMOS*$^{T1\text{-}Myc}$ mosaics (MYC) and in WT littermates (WT) at t3 ($n \geq 3$).

(D) EF and LV mass at t2 after a protocol of intense exercise from t0 to t2 (see Experimental Procedures).

(E) Heart/body weight ratios in the *iMOS*$^{T1\text{-}Myc}$ mosaics (MYC) and in WT littermates (WT) at t3 ($n \geq 3$).

(F and G) Confocal sections showing wheat germ agglutinin (WGA) staining to highlight cell perimeters in *iMOS*^{WT} (WT) (F) and *iMOS*$^{T1\text{-}Myc}$ (MYC) (G) mosaics at t3. Scale bar, 50 μm.

(H and I) Bright-field confocal section of cardiomyocytes isolated from *iMOS*^{WT} (WT) (H) and *iMOS*$^{T1\text{-}Myc}$ (MYC) (I) mosaic hearts at t3. Scale bar, 50 μm.

(J) Size (2D area) of cardiomyocytes shown in (H) and (I). $n \geq 4$ hearts and 236 cells.*$p < 0.1$; **$p < 0.05$; ***$p < 0.001$. Horizontal bars represent mean values.

(K and L) EYFP fluorescence intensity plotted against cell size for cardiomyocytes isolated from *iMOS*^{WT} (WT) (K) and *iMOS*$^{T1\text{-}Myc}$ (MYC) (L) mosaics. Lines in (K) and (L) represent the regression line ($R^2 = 2.040 \times 10^{-5}$ and 0.007204, respectively).

Data in (C)–(E) are means ± SEM.

correlation between these two parameters in either *iMOS*^{WT} or *iMOS*$^{T1\text{-}Myc}$ mosaic hearts (Figures 5K and 5L). These results show that sustained *Myc* overexpression from the *iMOS*$^{T1\text{-}Myc}$ allele during adult life does not provoke cardiomyocyte hypertrophy. Heart size and heart/body weight ratios were moreover similar in both mosaics, indicating that overall cardiac cellular and organ anatomy are preserved.

We next determined the proportions of cardiomyocyte populations at different times after mosaic induction. While in *iMOS*^{WT} hearts the proportion of EYFP cardiomyocytes was 53% at 1 year of age (Figures 6A and 6D), in the *iMOS*$^{T1\text{-}Myc}$ mosaics, the proportion increased progressively from a frequency similar to that found in *iMOS*^{WT} hearts to 66% at 1 year of age (Figures 6B and 6D). Interestingly, half of this enrichment took place during the first month of observation. Since there were no major changes in heart mass or cardiomyocyte size (Figures 5E and 5J), these observations suggest that *Myc*-overexpressing cardiomyocytes expand at the expense of WT cardiomyocytes during adult life. To directly test this, we determined the relative frequency of ECFP cardiomyocytes with respect to all fluorescent (ECFP+EYFP) cardiomyocytes in 1-year-old *iMOS*$^{T1\text{-}Myc}$ and *iMOS*^{WT} mosaics (Figures 6E–6H). The ECFP cell frequency was ~60% lower in the *iMOS*$^{T1\text{-}Myc}$ mosaics, confirming that the expansion of the Myc-overexpressing cardiomyocyte population is concomitant with a reduction in the WT population. Most adult cardiomyocytes in the mouse are tetraploid and contain two nuclei (Soonpaa et al., 1996); this, together with the partial recombination achieved by tamoxifen treatment, generates heterogeneous levels of *EYFP-Myc* content in cardiomyocytes, with a predicted predominance of cardiomyocytes with one or two active *EYFP-Myc* copies. We therefore refined our study to

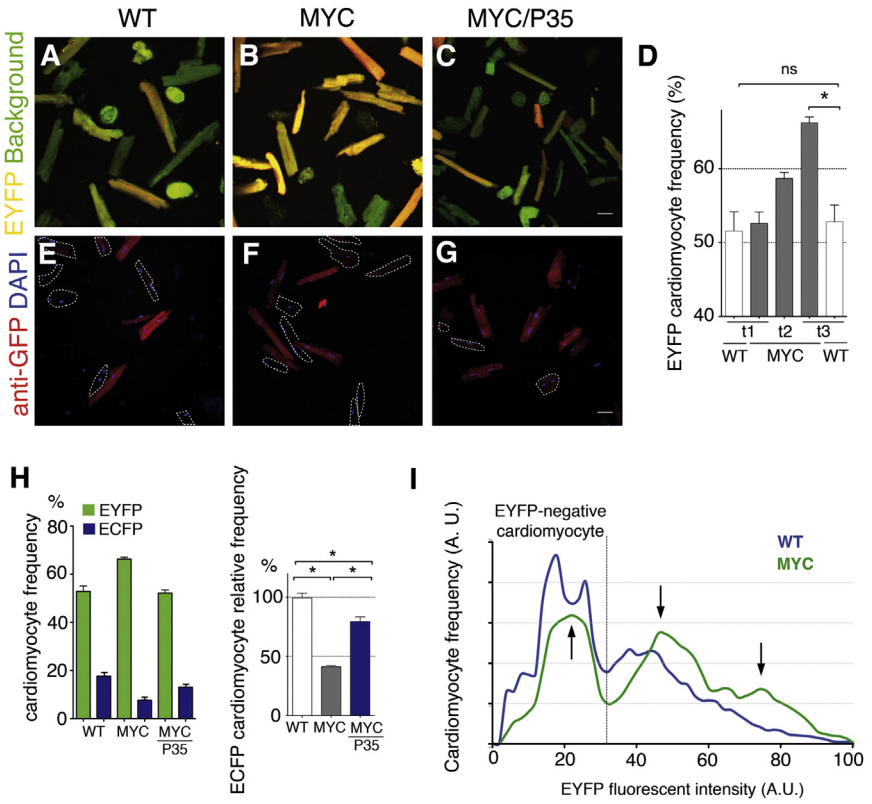

Figure 6. Myc Overexpression Induces Replacement of Adult Cardiomyocytes

(A–C) Confocal images of plated cardiomyocytes isolated at t3 (12 months after tamoxifen administration; see scheme in Figure 5) from *αMHCmerCremer*-recombined *iMOS*^{WT} (WT) (A), *iMOS*$^{T1\text{-}Myc}$ (MYC) (B), and *iMOS*$^{T1\text{-}Myc/T2\text{-}p35}$ (MYC/P35) (C) mosaics, showing native EYFP expression and background autofluorescence.

(D) Percentage of EYFP^{+} cardiomyocytes in cultures obtained from *αMHCmerCremer*-recombined *iMOS*^{WT} (WT) hearts at t1 and t3 and from *iMOS*$^{T1\text{-}Myc}$ (MYC) hearts at t1-t3 ($n \geq 3$ and 300 cells). Data are means ± SEM.

(E–G) Confocal images of plated cardiomyocytes obtained as in (A) –(C), showing anti-GFP immunofluorescence, which identifies EYFP^{+} and ECFP^{+} cardiomyocytes. Scale bar, 50 μm.

(H) Quantification of data represented in (A)–(G) at t3. The graph on the left shows the absolute frequencies of EYFP-Myc and ECFP-WT cardiomyocytes in *iMOS*^{WT} (WT), *iMOS*$^{T1\text{-}Myc}$ (MYC) and *iMOS*$^{T1\text{-}Myc/T2\text{-}p35}$ (MYC/P35) mosaics. In the graph on the right, the same data were expressed as relative ECFP^{+}/EYFP^{+} cardiomyocyte proportions relative to that observed in *iMOS*^{WT} (WT) mosaics, which was normalized to 100%.

(I) Graph represents the frequency of cardiomyocytes according to EYFP intensity in tamoxifen-induced *αMHCmerCremer*-recombined *iMOS*^{WT} (WT) and *iMOS*$^{T1\text{-}Myc}$ (MYC) mosaics, measured in cardiomyocytes isolated at t3, as in (A) –(C). The vertical dotted line marks the limit between background-fluorescent and EYFP-positive cardiomyocytes. Arrows indicate regions in which the frequencies overtly differ between the two mosaics studied. Data in bar graphs are means ± SEM. *$p < 0.05$ **$p < 0.01$ ***$p < 0.001$.

determine whether cardiomyocyte population expansion correlated with *EYFP-Myc* levels. Fluorescence was measured in isolated cardiomyocytes and the frequency of cells according to fluorescence intensity was determined (Figure 6I). This analysis showed that the enrichment in EYFP^{+} cardiomyocytes in *iMOS*$^{T1\text{-}Myc}$ mosaics mostly affects the populations with higher EYFP levels at the expense of EYFP-negative cardiomyocytes, whose frequency decreased (Figure 6I). These observations indicate a correlation between *Myc* dose levels and cardiomyocyte population prevalence in the adult myocardium.

Analysis of the Pathways Involved in Adult Cardiomyocyte Competition

To identify the pathways altered in the *iMOS*$^{T1\text{-}Myc}$ adult mosaic heart, we performed a transcriptomic analysis by RNA sequencing (RNA-seq), comparing 8-week old *iMOS*$^{T1\text{-}Myc}$ and control hearts (Figure S3). Among the genes more significantly up- or downregulated in *iMOS*$^{T1\text{-}Myc}$ hearts, there is a strong representation of genes involved in the response to cardiac overload, in cell growth/division, in energy metabolism, and in apoptosis (Figure S3A). Gene set enrichment analysis on all genes present in the RNA-seq experiment again detected the protective response to cardiac overload in *iMOS*$^{T1\text{-}Myc}$ hearts, including the activation of the atrial natriuretic peptide and fetal cardiomyocyte programs (Kishimoto et al., 2001; Kuhn et al., 2002) and the hepatocyte growth factor (HGF)/Rho/tissue remodeling pathways (Madonna et al., 2012). In contrast, the epidermal growth factor (EGF) pathway, involved in the development of pathological hypertrophy (Shah and Catt, 2003), was found repressed in *iMOS*$^{T1\text{-}Myc}$ hearts. Regarding metabolic processes, activation of the ribosome biosynthesis, a typical response to Myc overexpression, was also detected. In parallel, activation of the lysosomal pathway was as well present, indicating that metabolic activity was globally increased including both anabolic and catabolic processes. With regard to the metabolic processes, *iMOS*$^{T1\text{-}Myc}$ hearts showed a reduction in lipid catabolism and in assembly of the peroxisome, the main organelle for lipid catabolism, suggesting a modification in the fuel usage by Myc-overexpressing cardiomyocytes. A remarkable alteration was found in various regulators of the circadian rhythm; *Dbp* and *Per1*, *2*, and *3* were upregulated and *Arntl* (*Bmal1*) was downregulated. Circadian rhythm transcription factors are essential regulators of cardiac metabolism and regulate the balance between lipid and glucose usage in the heart and display a feedback regulation with the oxidative phosphorylation pathway in the heart (Durgan and Young, 2010). A major regulator of cardiac metabolism, AMP-activated protein kinase, has also been described to undergo circadian regulation (Tsai et al., 2010), its regulatory subunit is overexpressed in the *iMOS*$^{T1\text{-}Myc}$ hearts, and it can be activated by Myc overexpression (Nieminen et al., 2013). The results observed are therefore compatible with a modified metabolic status of the *iMOS*$^{T1\text{-}Myc}$

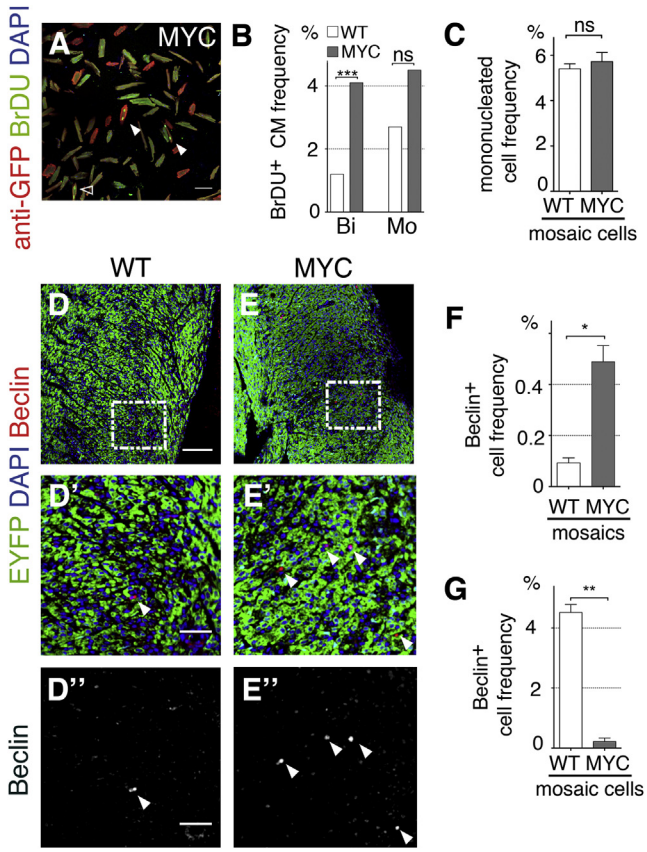

Figure 7. Analysis of Autophagy and BrdU Incorporation in Postnatal Hearts

(A) Confocal image of cardiomyocytes isolated from an *iMOS*$^{T1\text{-}Myc}$ adult heart showing GFP and BrdU staining. Arrowheads show BrdU^{+}/GFP^{+} mononucleated (empty arrowheads) and binucleated (filled arrowheads) cardiomyocytes. Scale bar, 50 μm.

(B) Graph showing the frequency of BrdU^{+} cardiomyocytes in the ECFP-WT (WT) and EYFP-Myc (MYC) populations of the *iMOS*$^{T1\text{-}Myc}$ adult hearts. Bi, binucleated; Mo, mononucleated.

(C) Graph showing the proportion of mononucleated cardiomyocytes within the ECFP-WT (WT) and EYFP-Myc (MYC) populations of the *iMOS*$^{T1\text{-}Myc}$ adult hearts. n = 4 hearts and >300 cells/heart.

(D and E) Confocal sections showing postnatal hearts from *iMOS*^{WT} (WT) (D) and *iMOS*$^{T1\text{-}Myc}$ (MYC) mosaics (E) showing Beclin-1 antibody staining together with iMOS cell populations mapping. Scale bar, 50 μm. (D′ and E′) Higher magnification of boxed areas in (D) and (E). Arrowheads point to Beclin^{+} cells. (D″ and E″) Beclin signal from (D′) and (E′) in isolation. Scale bar, 20 μm.

(F) Total Beclin^{+} cell frequency in *iMOS*^{WT} (WT) and *iMOS*$^{T1\text{-}Myc}$ (MYC) mosaics (n = 3 WT and 5 MYC).

(G) Beclin^{+} cell frequency within the ECFP-WT (ECFP) and EYFP-Myc cell populations (MYC) of the *iMOS*$^{T1\text{-}Myc}$ mosaics.

Graphs in (C), (F), and (G) show means ± SEM. *p < 0.1; **p < 0.05; ***p < 0.001. Statistical analysis in (B) was done using the χ^2 test. ns, not significant.

with either a direct or indirect impact of Myc overexpression on the circadian metabolic regulation. In agreement with this view, the Ingenuity Pathway analysis on the selected up- and downregulated genes (Figure S3B) indicates a modification of the lipid metabolism and a reduction of the oxidative phosphorylation activity in *iMOS*$^{T1\text{-}Myc}$ hearts. The top networks identified by this analysis for the upregulated, downregulated, and joint gene sets are again the networks activated in response to cardiac overload (Figures 3B and 3C). In agreement with these results, we found that the expression of the atrial natriuretic peptide was clearly activated in a patchy pattern in the ventricles of the *iMOS*$^{T1\text{-}Myc}$ mosaic hearts (Figure S3D).

Given the known functions of Myc in cardiomyocytes, the pathways detected likely result from cell-autonomous Myc functions and may relate to the ability of Myc-overexpressing cardiomyocytes to replace the WT cardiomyocyte population. In addition, the gene set enrichment study identified the activation of the apoptosis regulation and inflammation pathways in *iMOS*$^{T1\text{-}Myc}$ hearts, which could be related to the death and removal of WT cardiomyocytes. We therefore used the *iMOS*$^{T1\text{-}Myc/T2p35}$ mosaics to undertake a functional study of the involvement of cell death. This analysis showed that p35 expression largely rescues the ECFP cell population (Figures 6C, 6G, and 6H). These results indicate that adult cardiomyocytes undergo *Myc*-induced cell competition, which progresses by elimination of WT cardiomyocytes and their replacement by cardiomyocytes with high Myc levels. We then analyzed whether increased proliferation of the Myc-overexpressing population is contributing to this phenomenon. We found that BrdU incorporation was 4-fold more frequent in the EYFP-Myc cardiomyocytes than in the WT cardiomyocytes of *iMOS*$^{T1\text{-}Myc}$ mosaic hearts (Figure 7B). This increase did not alter the proportion of mononucleated cardiomyocytes (Figure 7C), suggesting that the balance between mononucleated cardiomyocyte division and binucleation is preserved.

To directly assess the involvement of apoptosis in the cardiomyocyte population shift, we analyzed the TUNEL pattern in adult *iMOS*$^{T1\text{-}Myc}$ mosaics; however, we found no significant differences in TUNEL frequency between the *EYFP-Myc* and *ECFP-WT* cell populations. These results suggested that, unlike the situation during development, apoptosis might not be involved in the elimination of WT cardiomyocytes in adults, despite the activation of apoptotic pathways detected by RNA-seq. We then explored whether alternative cell-death pathways could be operating in postnatal cardiomyocytes. Given that p35, in addition to inhibiting apoptotic cell death, can also inhibit autophagic cell death (Martin and Baehrecke, 2004) and that many apoptosis regulators are also involved in autophagic cell death, we tested whether this pathway could be involved in postnatal cardiomyocyte cell competition. Analysis of the autophagic death-specific marker Beclin (Liang et al., 1999) showed rare positive cells in *iMOS*^{WT} hearts (Figures 7D–7D″); however, the frequency of Beclin-positive cells increased by 5-fold in *iMOS*$^{T1\text{-}Myc}$ mosaic hearts (Figure 7E–7E″ and 7F). Moreover, the frequency of Beclin-positive cells within the *iMOS*$^{T1\text{-}Myc}$ mosaics was 9-fold higher in ECFP-WT cells than in EYFP-Myc cells (Figure 7G). These results indicate that autophagic cell death instead of apoptotic cell death is a major contributor to postnatal cardiomyocyte cell competition.

DISCUSSION

In this study, we demonstrate the ability of moderate Myc overexpression to induce cell competition in the developing and adult mouse heart. Previous studies showed that strong Myc

overexpression during fetal life leads to cardiac hyperplasia due to cardiomyocyte hyperproliferation, while overexpression in adults leads to cardiac hypertrophy due to cardiomyocyte overgrowth (Jackson et al., 1990; Xiao et al., 2001). In contrast, we found that the Myc overexpression levels provided by the endogenous promoter of the *Rosa26* locus do not lead to cardiac hypertrophy or hyperplasia. These results agree with previous evidence of ubiquitous $MycER^{T2}$ expression from the *Rosa26* locus, which did not induce cardiac hypertrophy even when two alleles were present (Murphy et al., 2008). A molecular signature typical of the response to cardiac overload however was activated. The activated pathways (Nppa, HGF) are cardioprotective and stimulate benign adaptation to increased cardiac function demands (Kishimoto et al., 2001; Kuhn et al., 2002; Madonna et al., 2012). In particular, the HGF pathway is not only involved in the cardiac overload response but also stimulates cardiac regeneration (Madonna et al., 2012). The activation of these pathways in the absence of cardiac overload, or in the presence of increased cardiac demand due to intense exercise, did not result in functional impairment. In fact, the EGF pathway, involved in pathological cardiac hypertrophy (Lee et al., 2011), was found inhibited in the Myc mosaic hearts. The Myc levels used here therefore can be considered ''homeostatic'' in the heart, since hearts exposed to these levels stay within normal anatomical and functional parameters. Interestingly, these expression levels provided in a mosaic fashion are enough to trigger cell competition, thereby enabling Myc-high cardiomyocytes to eliminate neighboring WT cardiomyocytes and expand to replace them. These results identify a window in which Myc level fluctuations can affect cardiomyocyte behavior to promote homeostatic changes in myocardial cell composition without affecting organ development and function.

These observations highlight the remarkable ability of fetal cardiomyocyte populations to undergo changes in composition without disrupting cardiac function. Previous studies showed that in mosaic hearts composed of wild-type cardiomyocytes and others carrying a deleterious mutation, the wild-type cardiomyocytes overproliferate during development to compensate for the loss of mutant cardiomyocytes (Drenckhahn et al., 2008). These studies indicate that the fetal heart bears sensing mechanisms that detect the loss of functional cardiomyocytes and promote their replacement. Our present results show that this replacement ability can also be stimulated by cell competition, whereby even undamaged wild-type cardiomyocytes can be eliminated and replaced by more competitive cells, without compromising cardiac homeostasis. Interestingly, this ability is retained during adult life, albeit at a notably slower pace with respect to that observed during development. In *Drosophila*, damaged postmitotic cells in the ovary can be eliminated and compensated for by hypertrophy of the remaining healthy cells (Tamori and Deng, 2013), while in the eye, postmitotic cells become refractory to cell competition (Tyler et al., 2007). Here, we found that, despite the predominant postmitotic nature of adult cardiomyocytes, the loss of the outcompeted population is not compensated by hypertrophy of winner cells but through overproliferation.

The mechanisms by which neighboring cells compare their fitness during cell competition in the mammalian embryo remain unknown, but a common theme of cell competition in the epiblast and the developing heart is the elimination of loser cells by apoptosis. In fact, in the fetal heart, we did not observe overt differences in proliferation between the two mosaic populations. This result is in apparent conflict with the fact that overexpansion of *Islet-Cre*-recombined cardiomyocyte population requires overproliferation and with the fact that the relative reduction of the WT cardiomyocyte population in the *Nkx2.5-Cre*-recombined mosaics requires compensatory proliferation to preserve normal heart size. The 5.7× expansion of the *IsletCre*-recombined population, however, involves only 2.5 extra cell cycles per cell in the 11 days between the activation of the driver at E7.5 and birth. This yields a total of 0.22 extra divisions per cell and day. In the case of the studies with the *Nkx2.5Cre* driver, between E8.5 and E11.5, a 60% reduction in the original 25% WT cardiomyocyte population was observed, which represents a 15% of the total cardiomyocyte population. To replace the 15% missing cardiomyocytes, only 0.15 extra cell divisions/cardiomyocyte would be required during the 3-day observation period. The degree of overproliferation required to explain the changes observed is therefore small and might not be experimentally detectable, especially since PHH3 and BrdU alone might not be enough for a full characterization of the cell proliferation rate cell proliferation.

In adult cardiomyocytes, however, we found a clear increase in the proliferative ability of winner cardiomyocytes, which likely contributes to the replacement of the loser population. While this increased proliferation capacity might be essential for the competitive ability, it is clearly not sufficient, and elimination of the loser population is still a requirement for cell competition in the adult heart. In fact, this overproliferation is most likely only compensatory for the loss of WT cardiomyocytes, since the homogeneous overexpression of two *ROSA26-MycER* copies does not lead to overproliferation in the adult heart (Murphy et al., 2008). The compensatory nature of this overproliferation would also explain the absence of cardiac overgrowth upon Myc mosaic overexpression.

These results suggest that fitness comparison between neighbors and death of the less-fit cells is a common theme in cell competition in very different scenarios. The fact that autophagic instead of apoptotic cell death is observed in adult cardiomyocytes could be more related to the specific features of adult cardiomyocytes than to the cell-competition phenomenon. Dying cells are normally eliminated by macrophages, but the size of an adult cardiomyocyte is about 100 times that of a macrophage, so a phase of self-destructive autophagy might be necessary before they can be eliminated by macrophages in a controlled manner. In fact, the typical example of autophagic death in *Drosophila* involves as well the elimination of giant cells of the salivary gland (Martin and Baehrecke, 2004). These considerations are in agreement with the predominance of TUNEL-negative autophagic cardiomyocyte death reported in heart failure patients (Knaapen et al., 2001).

The fact that cardiomyocytes undergo Myc-induced cell competition suggests that cell competition operates during normal heart development for the elimination of impaired cardiomyocytes unable to meet the anabolic rates demanded in the myocardium. Anabolism-induced cell competition thus appears

as a widespread phenomenon in mammalian tissues and not restricted to stem cell pools like the epiblast. There is an important difference, however, between endogenous cell competition in the epiblast and how it might operate during cardiogenesis: whereas epiblast development is characterized by a strong pattern of cell competition-associated apoptosis, during cardiogenesis, cardiomyocyte death is very infrequent (Poelmann et al., 2000). This suggests that while cell competition would work as a cell quality-control mechanism in both scenarios, in the epiblast it functions as a constitutive program, whereas during cardiogenesis it is used contingently, only if impaired cardiomyocytes appear. Since cardiomyocyte competition ability extends into adult life, it will be very interesting in the future to study whether cell competition is involved in maintaining tissue fitness during aging and whether it can contribute to natural or induced repair of cardiac insults in which cardiomyocytes are lost or impaired.

EXPERIMENTAL PROCEDURES

Mouse Strains

The *iMOS*^{WT}, *iMOS*$^{T1\text{-}Myc}$, and *iMOS*$^{T1\text{-}Myc/T2\text{-}p35}$ mouse lines have been described (Clavería et al., 2013). Here, they were used in combination with different Cre-expressing lines to induce genetic mosaics in the developing and adult mouse heart. Experimental embryos or born mice were generated from crosses of homozygous *iMOS* females with males carrying the different Cre drivers: *Nkx2.5Cre* (Stanley et al., 2002), *Islet1Cre* (Yang et al., 2006), and *αMHCmerCremer* (Sohal et al., 2001). Mice were genotyped by PCR (Clavería et al., 2013). To induce recombination in *iMOS*;*αMHCmerCremer* mice, they were fed for 1 month with pellets containing tamoxifen at 40 g/kg (Teklad ref. TD.07262).

Confocal Microscopy

Whole embryonic hearts or histological sections were imaged with a Nikon A1R confocal microscope using 405, 458, 488, 568, and 633 nm wavelengths and 20×/0.75 dry and 40×/1.30 oil objectives. Areas occupied by EYFP and ECFP cells were quantified using the threshold detection and particle analysis tools in ImageJ (NIH; http://rsb.info.nih.gov/ij). To calculate the relative frequency of ECFP cells, the percentage of ECFP area observed was divided by the average percentage in *iMOS*^{WT} mosaics. All percentages were normalized to a 100% value in the WT mosaic. ECFP was scored either by direct identification of native ECFP fluorescence or by subtracting the area of native EYFP from the anti-GFP staining, which detects both EYFP and ECFP.

Immunofluorescence and TUNEL Assay

Embryos were obtained at different days of gestation and fixed overnight at 4°C in 2% paraformaldehyde in PBS. Hearts were either dissected for whole-mount staining or gelatin embedded and cryosectioned. Adult cardiomyocytes were isolated by Langerdorff perfusion with liberase (Roche Applied Science) and plated for confocal imaging as described previously (García-Prieto et al., 2014). Primary antibodies used were anti-phosphohistone H3 (Ser 10), anti-Myc polyclonal antibody (Millipore), Living colors Rabbit polyclonal anti-GFP antibody (Clontech), Beclin1 (Cell Signaling), and Nppa (Millipore). Immunofluorescence was performed following standard procedures. TUNEL was performed on whole-mount embryonic hearts or sections using terminal deoxynucleotidyl transferase (TdT) and biotin-16-2′-deoxy-uridine-5′-triphosphate (Biotin-16-dUTP) (both from Roche), and developed with various streptavidin fluorescent conjugates (Jackson ImmunoResearch).

Statistical Analysis

To compare average percentages of ECFP cells/area between more than two groups, the Kruskal-Wallis test was used (assuming nonnormal distributions). For comparisons of two groups, a Mann-Whitney test was used. To test the correlation between cell size and EYFP expression, a linear regression model was used. All comparisons were made using Prism statistical analysis software. The significance of BrdU^{+} frequency and mononucleated cardiomyocyte frequency comparisons from adult hearts was analyzed using a proportions test as implemented in R.

ACCESSION NUMBERS

The NCBI Gene Expression Omnibus database accession number for the RNA-seq data reported in this paper is GSE58858.

SUPPLEMENTAL INFORMATION

Supplemental information includes Supplemental Experimental Procedures, three figures, and one movie and can be found with this article online at http://dx.doi.org/10.1016/j.celrep.2014.08.005.

ACKNOWLEDGMENTS

We thank J.L. de la Pompa for comments on the manuscript, V. García for mouse work, E. Arza and A.M. Santos for help with microscopy and 3D reconstruction, J. García-Prieto for help with cardiomyocyte isolation, A.V. Alonso for the echocardiography assays, F. Sánchez-Cabo for statistics, and S. Bartlett for text editing. The CNIC Genomics unit performed the RNA sequencing procedures. This work was supported by grants BFU2012-31086 and RD12/0019/0005 (ISCIII) from the Spanish Ministry of Economy and Competition (MINECO) and grant P2010/BMD-2315 from the Madrid Regional Government. C.V. is supported by a FPI grant from the MINECO. The CNIC is supported by the MINECO and the Pro-CNIC Foundation.

Received: February 5, 2014
Revised: April 21, 2014
Accepted: August 1, 2014
Published: September 4, 2014

REFERENCES

Baker, N.E. (2011). Cell competition. Curr. Biol. *21*, R11–R15.

Bondar, T., and Medzhitov, R. (2010). p53-mediated hematopoietic stem and progenitor cell competition. Cell Stem Cell *6*, 309–322.

Clavería, C., Albar, J.P., Serrano, A., Buesa, J.M., Barbero, J.L., Martínez-A, C., and Torres, M. (1998). Drosophila grim induces apoptosis in mammalian cells. EMBO J. *17*, 7199–7208.

Clavería, C., Giovinazzo, G., Sierra, R., and Torres, M. (2013). Myc-driven endogenous cell competition in the early mammalian embryo. Nature *500*, 39–44.

Dang, C.V. (2013). MYC, metabolism, cell growth, and tumorigenesis. Cold Spring Harb Perspect Med *3*.

Davis, A.C., Wims, M., Spotts, G.D., Hann, S.R., and Bradley, A. (1993). A null c-myc mutation causes lethality before 10.5 days of gestation in homozygotes and reduced fertility in heterozygous female mice. Genes Dev. *7*, 671–682.

de Beco, S., Ziosi, M., and Johnston, L.A. (2012). New frontiers in cell competition. Dev. Dyn. *241*, 831–841.

de la Cova, C., Abril, M., Bellosta, P., Gallant, P., and Johnston, L.A. (2004). Drosophila myc regulates organ size by inducing cell competition. Cell *117*, 107–116.

Drenckhahn, J.D., Schwarz, Q.P., Gray, S., Laskowski, A., Kiriazis, H., Ming, Z., Harvey, R.P., Du, X.J., Thorburn, D.R., and Cox, T.C. (2008). Compensatory growth of healthy cardiac cells in the presence of diseased cells restores tissue homeostasis during heart development. Dev. Cell *15*, 521–533.

Durgan, D.J., and Young, M.E. (2010). The cardiomyocyte circadian clock: emerging roles in health and disease. Circ. Res. *106*, 647–658.

Evans, S.M., Yelon, D., Conlon, F.L., and Kirby, M.L. (2010). Myocardial lineage development. Circ. Res. *107*, 1428–1444.

Gallant, P. (2013). Myc function in Drosophila. Cold Spring Harb Perspect Med *3*, a014324.

García-Prieto, J., García-Ruiz, J.M., Sanz-Rosa, D., Pun, A., García-Alvarez, A., Davidson, S.M., Fernández-Friera, L., Nuno-Ayala, M., Fernández-Jiménez, R., Bernal, J.A., et al. (2014). β3 adrenergic receptor selective stimulation during ischemia/reperfusion improves cardiac function in translational models through inhibition of mPTP opening in cardiomyocytes. Basic Res. Cardiol. *109*, 422.

Hay, B.A., Wolff, T., and Rubin, G.M. (1994). Expression of baculovirus P35 prevents cell death in Drosophila. Development *120*, 2121–2129.

Hurlin, P.J. (2013). Control of vertebrate development by MYC. Cold Spring Harb Perspect Med *3*, a014332.

Jackson, T., Allard, M.F., Sreenan, C.M., Doss, L.K., Bishop, S.P., and Swain, J.L. (1990). The c-myc proto-oncogene regulates cardiac development in transgenic mice. Mol. Cell. Biol. *10*, 3709–3716.

Kelly, R.G., Brown, N.A., and Buckingham, M.E. (2001). The arterial pole of the mouse heart forms from Fgf10-expressing cells in pharyngeal mesoderm. Dev. Cell *1*, 435–440.

Kishimoto, I., Rossi, K., and Garbers, D.L. (2001). A genetic model provides evidence that the receptor for atrial natriuretic peptide (guanylyl cyclase-A) inhibits cardiac ventricular myocyte hypertrophy. Proc. Natl. Acad. Sci. USA *98*, 2703–2706.

Knaapen, M.W., Davies, M.J., De Bie, M., Haven, A.J., Martinet, W., and Kockx, M.M. (2001). Apoptotic versus autophagic cell death in heart failure. Cardiovasc. Res. *51*, 304–312.

Kuhn, M., Holtwick, R., Baba, H.A., Perriard, J.C., Schmitz, W., and Ehler, E. (2002). Progressive cardiac hypertrophy and dysfunction in atrial natriuretic peptide receptor (GC-A) deficient mice. Heart *87*, 368–374.

Lee, K.S., Park, J.H., Lim, H.J., and Park, H.Y. (2011). HB-EGF induces cardiomyocyte hypertrophy via an ERK5-MEF2A-COX2 signaling pathway. Cell. Signal. *23*, 1100–1109.

Levayer, R., and Moreno, E. (2013). Mechanisms of cell competition: themes and variations. J. Cell Biol. *200*, 689–698.

Levens, D. (2013). Cellular MYCro economics: Balancing MYC function with MYC expression. Cold Spring Harb Perspect Med *3*.

Liang, X.H., Jackson, S., Seaman, M., Brown, K., Kempkes, B., Hibshoosh, H., and Levine, B. (1999). Induction of autophagy and inhibition of tumorigenesis by beclin 1. Nature *402*, 672–676.

Madonna, R., Cevik, C., Nasser, M., and De Caterina, R. (2012). Hepatocyte growth factor: molecular biomarker and player in cardioprotection and cardiovascular regeneration. Thromb. Haemost. *107*, 656–661.

Martin, D.N., and Baehrecke, E.H. (2004). Caspases function in autophagic programmed cell death in Drosophila. Development *131*, 275–284.

Marusyk, A., Porter, C.C., Zaberezhnyy, V., and DeGregori, J. (2010). Irradiation selects for p53-deficient hematopoietic progenitors. PLoS Biol. *8*, e1000324.

Morata, G., and Ripoll, P. (1975). Minutes: mutants of Drosophila autonomously affecting cell division rate. Dev. Biol. *42*, 211–221.

Moreno, E., and Basler, K. (2004). dMyc transforms cells into super-competitors. Cell *117*, 117–129.

Murphy, D.J., Junttila, M.R., Pouyet, L., Karnezis, A., Shchors, K., Bui, D.A., Brown-Swigart, L., Johnson, L., and Evan, G.I. (2008). Distinct thresholds govern Myc's biological output in vivo. Cancer Cell *14*, 447–457.

Nieminen, A.I., Eskelinen, V.M., Haikala, H.M., Tervonen, T.A., Yan, Y., Partanen, J.I., and Klefström, J. (2013). Myc-induced AMPK-phospho p53 pathway activates Bak to sensitize mitochondrial apoptosis. Proc. Natl. Acad. Sci. USA *110*, E1839–E1848.

Poelmann, R.E., Molin, D., Wisse, L.J., and Gittenberger-de Groot, A.C. (2000). Apoptosis in cardiac development. Cell Tissue Res. *301*, 43–52.

Rana, M.S., Christoffels, V.M., and Moorman, A.F. (2013). A molecular and genetic outline of cardiac morphogenesis. Acta Physiol. (Oxf.) *207*, 588–615.

Sancho, M., Di-Gregorio, A., George, N., Pozzi, S., Sánchez, J.M., Pernaute, B., and Rodríguez, T.A. (2013). Competitive interactions eliminate unfit embryonic stem cells at the onset of differentiation. Dev. Cell *26*, 19–30.

Shah, B.H., and Catt, K.J. (2003). A central role of EGF receptor transactivation in angiotensin II -induced cardiac hypertrophy. Trends Pharmacol. Sci. *24*, 239–244.

Sohal, D.S., Nghiem, M., Crackower, M.A., Witt, S.A., Kimball, T.R., Tymitz, K.M., Penninger, J.M., and Molkentin, J.D. (2001). Temporally regulated and tissue-specific gene manipulations in the adult and embryonic heart using a tamoxifen-inducible Cre protein. Circ. Res. *89*, 20–25.

Soonpaa, M.H., Kim, K.K., Pajak, L., Franklin, M., and Field, L.J. (1996). Cardiomyocyte DNA synthesis and binucleation during murine development. Am. J. Physiol. *271*, H2183–H2189.

Stanley, E.G., Biben, C., Elefanty, A., Barnett, L., Koentgen, F., Robb, L., and Harvey, R.P. (2002). Efficient Cre-mediated deletion in cardiac progenitor cells conferred by a 3'UTR-ires-Cre allele of the homeobox gene Nkx2-5. Int. J. Dev. Biol. *46*, 431–439.

Tamori, Y., and Deng, W.M. (2013). Tissue repair through cell competition and compensatory cellular hypertrophy in postmitotic epithelia. Dev. Cell *25*, 350–363.

Tsai, J.Y., Kienesberger, P.C., Pulinilkunnil, T., Sailors, M.H., Durgan, D.J., Villegas-Montoya, C., Jahoor, A., Gonzalez, R., Garvey, M.E., Boland, B., et al. (2010). Direct regulation of myocardial triglyceride metabolism by the cardiomyocyte circadian clock. J. Biol. Chem. *285*, 2918–2929.

Tyler, D.M., Li, W., Zhuo, N., Pellock, B., and Baker, N.E. (2007). Genes affecting cell competition in Drosophila. Genetics *175*, 643–657.

Vincent, S.D., and Buckingham, M.E. (2010). How to make a heart: the origin and regulation of cardiac progenitor cells. Curr. Top. Dev. Biol. *90*, 1–41.

Vincent, J.P., Fletcher, A.G., and Baena-Lopez, L.A. (2013). Mechanisms and mechanics of cell competition in epithelia. Nat. Rev. Mol. Cell Biol. *14*, 581–591.

Xiao, G., Mao, S., Baumgarten, G., Serrano, J., Jordan, M.C., Roos, K.P., Fishbein, M.C., and MacLellan, W.R. (2001). Inducible activation of c-Myc in adult myocardium in vivo provokes cardiac myocyte hypertrophy and reactivation of DNA synthesis. Circ. Res. *89*, 1122–1129.

Yang, L., Cai, C.L., Lin, L., Qyang, Y., Chung, C., Monteiro, R.M., Mummery, C.L., Fishman, G.I., Cogen, A., and Evans, S. (2006). Isl1Cre reveals a common Bmp pathway in heart and limb development. Development *133*, 1575–1585.